

# Effects of Relativistic Thermal Velocity Spread of Beam on Electromagnetic Instabilities in Fast Ignition

Peiyong YE and Katsunobu NISHIHARA

*Institute of Laser Engineering, Osaka University, Osaka 565-0871, Japan*

(Received 1 October 2007 / Accepted 1 November 2007)

We investigate the linear instability of electromagnetic modes caused by the interaction of a relativistic electron beam with a dense plasma, taking into account the relativistic thermal spread of the beam. To obtain a linear dispersion relation, the relativistic factor  $\gamma$  of the beam is expanded within the first order of the beam thermal spread. We show that growth rate becomes large when the relativistic thermal spread of the beam is taken into account. In addition, we discuss the effects of the relativistic beam thermal spread on growth rate and the wave number vector that yields the maximum growth.

© 2007 The Japan Society of Plasma Science and Nuclear Fusion Research

Keywords: fast ignition, beam-plasma system, electromagnetic instability, relativistic effect, energy transport

DOI: 10.1585/pfr.2.049

The fast-ignition scenario (FIS) involves interaction between a high-energy electron beam and a dense target plasma [1]. FIS requires the intense electron beam to propagate into the dense plasma to heat the fuel and to ignite fusion burning. In such a beam-plasma system, microscopic instability is one of the potential effects that may prevent energy transport of the beam electrons. Therefore, it is important to understand this interaction. Over the last few years, many studies have been conducted on the instability effects—both electromagnetic and electrostatic—of the interaction, in case of the FIS [2–4]. Electromagnetic instability is called Weibel instability [5], while electrostatic instability is known as two-stream instability [6]. Some studies have highlighted the necessity of analyzing the mixing of electromagnetic and electrostatic modes [2, 7], while other studies have shown the effects of nonrelativistic thermal spreads of a beam and background plasma on the growth rate of the instabilities [3, 4]. This paper is mainly concerned with the effects of the relativistic thermal spread of beam electrons on electromagnetic instabilities. Our 3D PIC simulations [8] show that the thermal spread of the beam electrons is not small enough to be neglected. We therefore expand the relativistic factor  $\gamma = \sqrt{1 - v^2/c^2}$  of the beam electrons to the first order of the thermal spread, which is different from that undertaken in previous works. Here,  $c$  and  $v$  are the speeds of light and electrons, respectively.

We consider a situation, shown in Fig. 1, where beam electrons with an average velocity of  $v_{b,x0}$  propagate in the  $x$  direction and background plasma electrons propagate in the direction opposite to the beam drift velocity with  $-v_{p,x0}$  to satisfy the current neutrality,  $n_b v_{b,x0} = n_p v_{p,x0}$ . Here,  $n_i$  ( $i = b$  or  $p$ ) is electron density, and the subscripts  $b$  and  $p$

denote the beam and background plasma, respectively. To emphasize the relativistic effect, we use relativistic velocity  $u_{b,x0}$  instead of  $v_{b,x0}$  in the figure. Here,  $\mathbf{u} = \gamma\mathbf{v}$ . Here, we consider the interaction of the relativistic hot beam with the nonrelativistic hot background plasma, neglect ion motion, and restrict ourselves to homogenous, spatially infinite, collisionless plasma.

We study the dynamics of the beam-plasma system using the relativistic Vlasov equation and Maxwell equations:

$$\frac{\partial f}{\partial t} + \frac{\mathbf{u}}{\gamma} \cdot \frac{\partial f}{\partial \mathbf{r}} - \frac{e}{m_e} \left( \mathbf{E} + \frac{\mathbf{u}}{\gamma} \times \mathbf{B} \right) \cdot \frac{\partial f}{\partial \mathbf{u}} = 0, \quad (1)$$

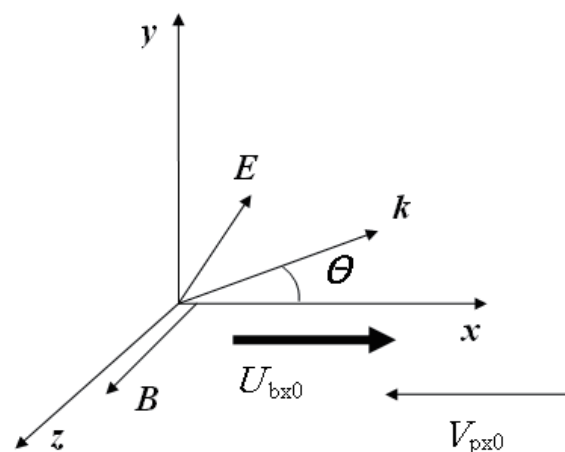


Fig. 1 Geometry of problem.  $u_{b,x0}$  is relativistic drift velocity of beam, and  $v_{p,x0}$  is nonrelativistic drift velocity of background plasma. Wave vector  $\mathbf{k}$  and electric field  $\mathbf{E}$  are in  $x$ - $y$  plane, and magnetic field  $\mathbf{B}$  is along  $z$  direction.  $\theta$  is angle between  $\mathbf{k}$  and  $x$  axis.

$$\nabla \times \mathbf{B} = \mathbf{j} + \varepsilon_0 \frac{\partial \mathbf{E}}{\partial t}, \quad \nabla \times \mathbf{E} = -\frac{\partial \mathbf{B}}{\partial t}, \quad (2)$$

$$\mathbf{j}(t, \mathbf{r}) = -e \int \frac{\mathbf{u}}{\gamma} f(t, \mathbf{r}, \mathbf{u}) d^3 u, \quad (3)$$

where  $f = f(t, \mathbf{r}, \mathbf{u})$  denotes the velocity distribution function of the beam and background plasma, and  $e$ ,  $m_e$ , and  $\varepsilon_0$  are electron charge, electron mass, and vacuum permittivity, respectively. We consider the electromagnetic perturbations to be of the form  $(\delta E_x, \delta E_y, \delta B_z, \delta j_x, \delta j_y, \delta f) \exp(ik_x x + ik_y y - i\omega t)$  with electric field  $\mathbf{E}$  and wave vector  $\mathbf{k}$  in the  $x$ - $y$  plane, and magnetic field  $\mathbf{B}$  in the  $z$  direction, as shown in Fig. 1. It should be noted that the electric and magnetic field modes are neither purely electrostatic nor purely electromagnetic. From Eqs. (1)–(3), we can derive a linear dispersion relation for the perturbations propagating in every possible direction from 0 to  $\pi/2$  in the  $x$ - $y$  plane, as

$$\begin{aligned} & \left(1 - \frac{k_x^2}{\omega^2} - \sum_i \frac{\omega_{pi}^2}{\omega^2} \varepsilon_{iyiy}\right) \left(1 - \frac{k_y^2}{\omega^2} - \sum_i \frac{\omega_{pi}^2}{\omega^2} \varepsilon_{ixxx}\right) \\ &= \left(\frac{k_x k_y}{\omega^2} - \sum_i \frac{\omega_{pi}^2}{\omega^2} \varepsilon_{ixiy}\right)^2, \end{aligned} \quad (4)$$

where

$$\varepsilon_{ilm} \equiv \omega \int \frac{u_l \Delta f_{0im}}{\omega - \mathbf{k} \cdot \mathbf{u} / \gamma} d^3 u, \quad (l, m \equiv x, y), \quad (5)$$

$$\begin{aligned} \Delta f_{0ix} &\equiv \frac{\partial f_{0i}}{\partial u_x} - \frac{k_y}{\omega} \left( \frac{\partial f_{0i}}{\partial u_x} u_y - \frac{\partial f_{0i}}{\partial u_y} u_x \right), \\ \Delta f_{0iy} &\equiv \frac{\partial f_{0i}}{\partial u_y} - \frac{k_x}{\omega} \left( \frac{\partial f_{0i}}{\partial u_y} u_x - \frac{\partial f_{0i}}{\partial u_x} u_y \right). \end{aligned} \quad (6)$$

We normalized time to  $1/\omega_p$  and space to the collisionless skin depth of  $c/\omega_p$ , where  $\omega_p$  is plasma frequency such that  $\omega_p^2 = e^2 n_p / (m_e \varepsilon_0)$ .

We use a simple waterbag velocity distribution function for the beam and background plasma:

$$\begin{aligned} f_{0i} &= \frac{n_i}{4v_{i\perp 0}^2 \cdot 2v_{i\parallel 0}} [\Theta(v_y + v_{i\perp 0}) - \Theta(v_y - v_{i\perp 0})] \\ &\times [\Theta(v_z + v_{i\perp 0}) - \Theta(v_z - v_{i\perp 0})] \\ &\times [\Theta(v_x \pm v_{ix0} + v_{i\parallel 0}) - \Theta(v_x \pm v_{ix0} - v_{i\parallel 0})]. \end{aligned} \quad (7)$$

Here,  $v_{i\parallel 0}$  is the thermal velocity spread in the  $x$  direction (parallel spread),  $v_{i\perp 0}$  is the thermal velocity spread in the  $y$  and  $z$  directions (perpendicular spread), and  $\Theta(x)$  is a step function. In Eq. (7), the minus and plus signs signify the beam and the background plasma, respectively.

By substituting Eq. (7) into Eqs. (5) and (6), we obtain Eq. (8), as shown below. Here, we have expanded the relativistic factor  $\gamma$  in Eq. (5) to the first order of the beam thermal spread relative to the beam drift velocity, i.e.,  $\gamma = \gamma_0 + u_{bx0} v_{b\parallel} / \gamma_0$ , where  $\gamma_0 = \sqrt{1 + u_{bx0}^2 / c^2}$ , in the velocity integration. Here,  $v_{b\parallel}$  is  $x$ -component of the beam velocity corresponding to the thermal spread. It should be noted that the perpendicular velocity spread,  $v_{b\perp 0}$ , appears

only in the second order in the relativistic factor.

$$\begin{aligned} & \sum_i \frac{\omega_{pi}^2}{\omega^2} \varepsilon_{ixxx} \\ &= \frac{-\alpha \omega_p^2 (\omega^2 + k_y^2 u_{bx0}^2)}{\omega^2 \gamma_0 ((\omega \gamma_0 - k_x u_{bx0})^2 - k_y^2 v_{b\perp 0}^2 - (k_x c - \omega \beta)^2 v_{b\parallel 0}^2 / c^2)} \\ &\quad - \frac{\omega_p^2 (\omega^2 + k_y^2 v_{px0}^2)}{\omega^2 ((\omega + k_x v_{px0})^2 - k_y^2 v_{p\perp 0}^2 - k_x^2 v_{p\parallel 0}^2)}, \end{aligned} \quad (8a)$$

$$\begin{aligned} & \sum_i \frac{\omega_{pi}^2}{\omega^2} \varepsilon_{iyiy} \\ &= \frac{-\alpha \omega_p^2 (\omega \gamma_0 - k_x u_{bx0})^2}{\omega^2 \gamma_0 ((\omega \gamma_0 - k_x u_{bx0})^2 - k_y^2 v_{b\perp 0}^2 - (k_x c - \omega \beta)^2 v_{b\parallel 0}^2 / c^2)} \\ &\quad - \frac{\omega_p^2 \cdot (\omega + k_x v_{px0})^2}{\omega^2 ((\omega + k_x v_{px0})^2 - k_y^2 v_{p\perp 0}^2 - k_x^2 v_{p\parallel 0}^2)}, \end{aligned} \quad (8b)$$

$$\begin{aligned} & \sum_i \frac{\omega_{pi}^2}{\omega^2} \varepsilon_{ixiy} \\ &= \frac{-\alpha \omega_p^2 k_y u_{bx0} (\omega \gamma_0 - k_x u_{bx0})}{\omega^2 \gamma_0 ((\omega \gamma_0 - k_x u_{bx0})^2 - k_y^2 v_{b\perp 0}^2 - (k_x c - \omega \beta)^2 v_{b\parallel 0}^2 / c^2)} \\ &\quad + \frac{\omega_p^2 \cdot k_y v_{px0} \cdot (\omega + k_x v_{px0})}{\omega^2 ((\omega + k_x v_{px0})^2 - k_y^2 v_{p\perp 0}^2 - k_x^2 v_{p\parallel 0}^2)}. \end{aligned} \quad (8c)$$

Here,  $\alpha = n_b / n_p$  and  $\beta = v_{bx0} / c$ . If we neglect the thermal spread effect in the relativistic factor in Eq. (5), that is, if  $\gamma = \gamma_0$  is substituted, then the term  $(k_x c - \omega \beta)^2 v_{b\parallel 0}^2 / c^2$  in Eq. (8) should be replaced with  $k_x^2 v_{b\parallel 0}^2$ . By substituting Eq. (8) into Eq. (4), we can obtain a dispersion relation. Hereafter, we call the growth rate obtained from Eq. (8) as the first-order relativistic factor (RF) solution, and the growth rate used with the constant relativistic factor  $\gamma_0$  in Eq. (5) as the constant RF solution. For the convenience of analyzing the instabilities, we use as parameters the dimensionless variables

$$\rho_{b\parallel, \perp 0} = \frac{v_{b\parallel, \perp 0}}{v_{bx0}}, \quad \rho_{p\parallel, \perp 0} = \frac{v_{p\parallel, \perp 0}}{v_{bx0}} \quad (9)$$

in addition to  $\alpha$  and  $\beta$ .

Figure 2 shows the growth rate of the instability in  $\mathbf{k}$  space. Here, we have normalized the wave number and growth rate as  $K_x = k_x v_{bx0} / \omega_p$ ,  $K_y = k_y v_{bx0} / \omega_p$  and  $\sigma = \text{Im}[\omega / \omega_p]$ , respectively. The two figures in Fig. 2 (a) correspond to a constant RF solution in  $\mathbf{k}$  space, while two figures in Fig. 2 (b) are those for a first-order RF solution. Here,  $\alpha = 0.05$  is used, which is fixed throughout the paper, and the other parameters are described in the figure caption. Even though these two sets of figures are similar to each other, it is easy to distinguish them. As Fig. 2 indicates, there exist two instabilities in different  $k$ -branches. One is the instability within a branch with small  $K_x < 1$ , and the other is that with a relatively large  $K_x$ . Hereafter,

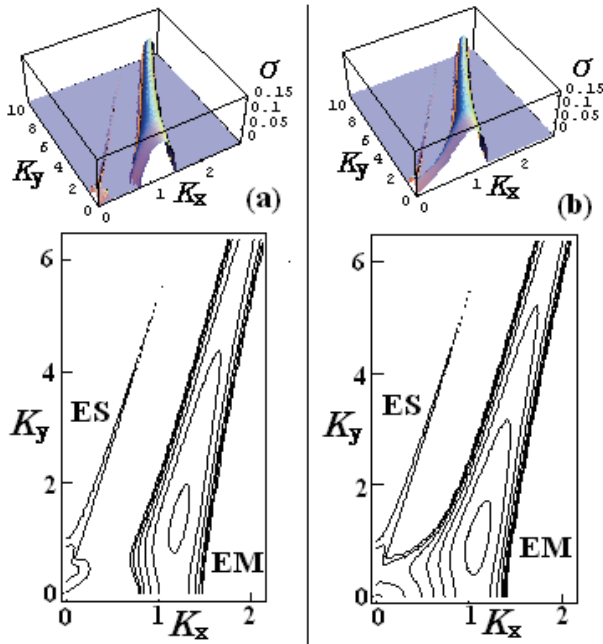


Fig. 2 Growth rate in  $K_x$ - $K_y$  plane with  $u_{bx0}/c = 1$ ,  $\rho_{b||0} = 0.3$ ,  $\rho_{b\perp 0} = 0.2$ , and  $\rho_{p||, \perp 0} = 0.05$ . (a) Constant RF solution. (b) First-order RF solution. Maximum contour lines are (a)  $\sigma = 0.135$  and (b)  $0.155$ , decreasing at rates of (a)  $0.016$  and (b)  $0.025$ . Maximum growth rates are about (a)  $\sigma = 0.139$  and (b)  $0.162$ .

we refer to the former branch as Branch EM and the latter as Branch ES, as shown in Fig. 2. The branches in  $k$  space separate from each other in the constant RF solution. However, the two branches in  $k$  space are connected to each other in the first-order RF solution. We can evaluate the mixing of electromagnetic and electrostatic modes by calculating  $|\mathbf{k} \cdot \mathbf{E}|/(|\mathbf{k}||\mathbf{E}|)$  for the electrostatic component and  $|\mathbf{k} \times \mathbf{E}|/(|\mathbf{k}||\mathbf{E}|)$  for the electromagnetic component. We find that the Branch EM consists mostly of the electromagnetic mode, while the Branch ES is mostly electrostatic. The Branches EM and ES correspond to the Weibel and two-stream instabilities, respectively. The mode continuously changes from electromagnetic to electrostatic as the  $x$ -component of the wave number  $K_x$  increases from 0 to 1. That is, the two modes combine in a certain  $K_x$  region between  $K_x = 0$  and  $K_x = 1$ . The growth rate of the two-stream instability is much larger than that of the Weibel instability for the parameters used.

The growth rate shown in Fig. 2(b) is re-plotted in the  $|K|$ - $\theta$  plane in Fig. 3, where  $\theta = \arctan(K_y/K_x)$ . The most unstable mode of the two-stream instability propagates obliquely at about 45 degrees with respect to the beam propagation direction when  $|K|$  is about 1.5. On the other hand, the most unstable mode of the Weibel instability occurs in the perpendicular direction when  $|K| \approx 0.5$ .

We now discuss the dependence of the maximum growth rate on beam velocity and thermal velocity spread. The maximum growth rate corresponds to the two-stream

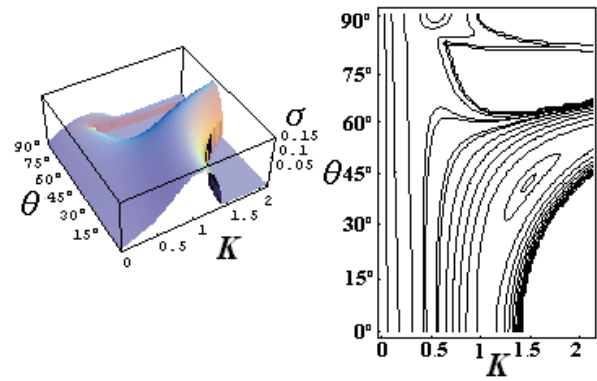


Fig. 3 Growth rate in  $|K|$ - $\theta$  space. Parameters are same as those in Fig. 2 (b).

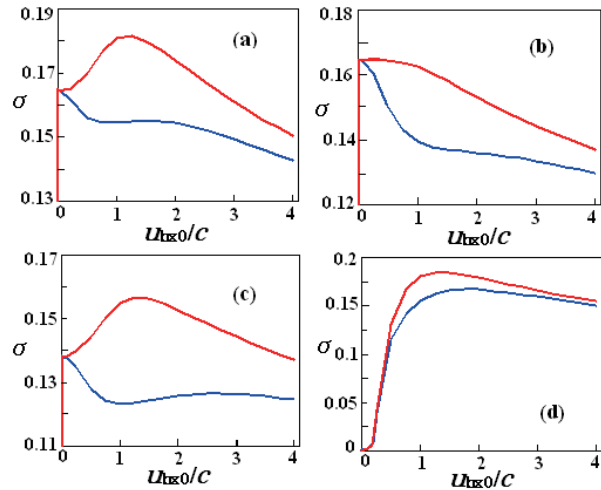


Fig. 4 Dependence of instability growth rate on beam velocity, first-order RF solution (red line), and constant RF solution (blue line). Parameters are (a)  $\rho_{b||0} = 0.3$ ,  $\rho_{b\perp 0} = 0.1$ ; (b)  $\rho_{b||0} = 0.3$ ,  $\rho_{b\perp 0} = 0.2$ ; (c)  $\rho_{b||0} = 0.4$ ,  $\rho_{b\perp 0} = 0.2$ ; (d)  $v_{b||0} = 0.21c$ ,  $v_{b\perp 0} = 0.07c$ , and  $v_{p||, \perp 0} = 0.035c$ ; and for (a), (b), and (c),  $\rho_{p||, \perp 0} = 0.05$ .

instability; Figure 4 shows its dependence on beam velocity at various thermal velocities. We also compare the maximum growth rates between the constant (blue) and the first-order (red) RF solutions. In Figs. 4(a)–(c), the ratios of the thermal velocity spread to the beam drift velocity are fixed, while in Fig. 4(d), those for the thermal velocity are fixed. For the fixed thermal spread, as shown in Fig. 4(d), the growth rate decreases uniformly to zero as the beam drift velocity for  $u_{bx0}/c < 1$  decreases. By including relativistic thermal spread in the relativistic factor, we obtain larger growth rates compared to the constant RF solutions in all cases. The difference between the two solutions becomes very large for beam drift velocity near  $u_{bx0} = c$ . The largest growth rate of the first-order RF solution does not simply decrease as the beam velocity  $v_{bx0}$  decreases, as

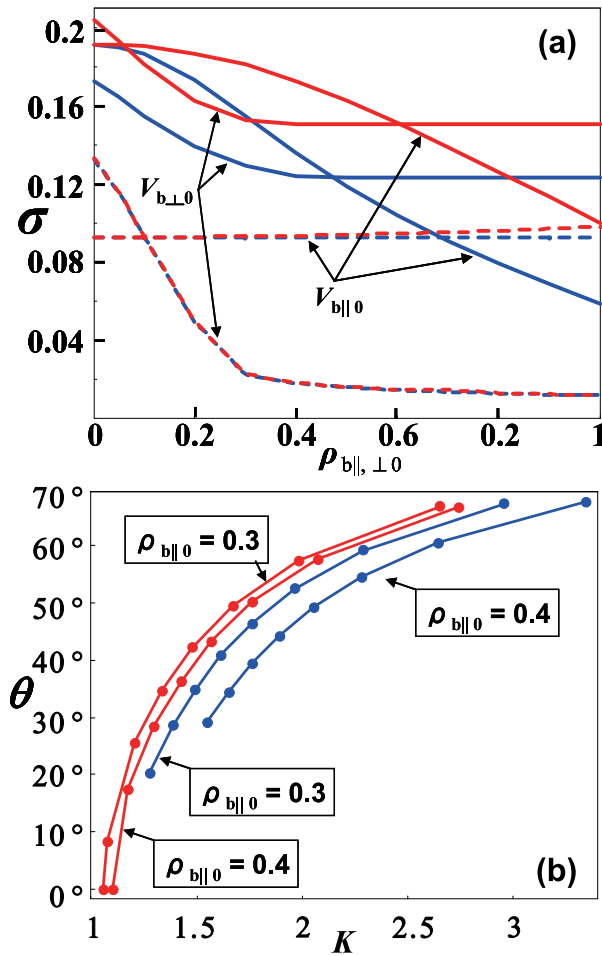


Fig. 5 (a) Dependence of maximum growth rate of electrostatic (solid line) and electromagnetic (dashed line) instabilities on beam thermal spread; first-order RF solution (red), and constant RF solution (blue). Fixed parameters are  $u_{bx0}/c = 1$ ,  $\rho_{b\parallel 0} = 0.3$ ,  $\rho_{b\perp 0} = 0.1$ , and  $\rho_{p\parallel,\perp 0} = 0.05$ . (b) Dependence of wave number  $|K|$  and propagation angle  $\theta$  on perpendicular thermal spread;  $\rho_{b\perp 0}$  varies from 0.05 to 0.4 from right to left with increments of 0.05. Fixed values of  $\rho_{b\parallel 0}$  are shown in figure.

shown in Fig. 4 (a) and (c).

Figure 5 (a) shows the dependence of the maximum growth rates on the beam thermal spread,  $\rho_{b\parallel 0}$  and  $\rho_{b\perp 0}$ , for electrostatic and electromagnetic instabilities. Here, we fixed beam drift velocity at  $u_{bx0}/c = 1$ . The maximum growth rate of the two-stream instability decreases as the

parallel thermal spread increases. However, the decrease of the first-order RF solution is very small up to  $\rho_{b\parallel 0} < 0.4$ , compared to that of the constant RF solution. The difference between the two solutions increases as  $\rho_{b\parallel 0}$  increases up to  $\rho_{b\parallel 0} < 0.6$ . The maximum growth rate also decreases as  $\rho_{b\perp 0}$  increases up to  $\rho_{b\perp 0} < 0.4$ . For the electromagnetic instability, the growth rate does not depend on the parallel spread, and there is also no difference between the two solutions. However, its growth rate decreases strongly as the perpendicular spread increases up to approximately  $\rho_{b\perp 0} < 0.3$ , and remains almost constant for large  $\rho_{b\perp 0}$ .

We have also investigated the dependence of the wave number vector responsible for the maximum growth rate on the beam thermal spread. The wave number  $|K|$  varies from  $|K| \approx 2.5$  to 1 and the propagation angle  $\theta$  varies from  $\approx 70$  to 0 degrees as  $\rho_{b\perp 0}$  increases from 0.05 to 0.4, as shown in Fig. 5 (b). The perpendicular spread strongly affects the propagation direction of the instability. However, we observed that the parallel spread does not greatly affect either  $|K|$  or  $\theta$ .

We have investigated the effects of relativistic beam thermal spread on electromagnetic instability in the interaction of a relativistic beam with dense plasma. We showed that, by taking into account relativistic thermal spread, the maximum growth rates become larger than those previously attained. We have also investigated the dependence of the growth rate and wave number vector responsible for the maximum growth on relativistic thermal velocity spread, and we found that the growth rate does not decrease significantly even for a relatively large thermal spread. In addition, it was noted that the propagation angle of the most unstable mode strongly depends on the thermal spread.

- [1] M. Tabak *et al.*, Phys. Plasma **1**, 1626 (1994).
- [2] L.O. Silva, R.A. Fonseca, J.W. Tonge, W.B. Mori and J.M. Dawson, Phys. Plasma **9**, 2458 (2001).
- [3] A. Bret, M.-C. Firpo and C. Deutsch, Phys. Rev. E **70**, 046401 (2004).
- [4] A. Bret, M.-C. Firpo and C. Deutsch, Phys. Rev. E **72**, 016403 (2005).
- [5] E.S. Weibel, Phys. Rev. Lett. **2**, 83 (1959).
- [6] O. Buneman, Phys. Rev. **115**, 503 (1959).
- [7] M. Tatarakis *et al.*, Phys. Rev. Lett. **90**, 175001 (2003).
- [8] Y. Danno, P. Ye and K. Nishihara, *Annual Progress Report* (ILE, Osaka Univ., 2007) p.123.